

PAPER

High frequency pulsed electrohydrodynamic printing with controllable fine droplets

To cite this article: Xin Yuan and Zhenhua Xiong 2018 *J. Micromech. Microeng.* **28** 095008

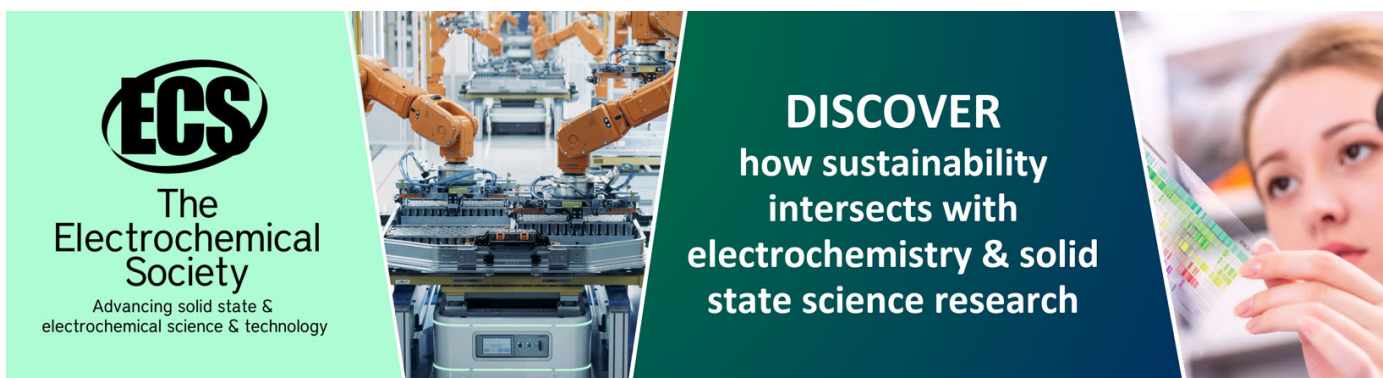
View the [article online](#) for updates and enhancements.

You may also like

- [Fine droplet generation using tunable electrohydrodynamic pulsation](#)
Xin Yuan, Zhengyu Ba and Zhenhua Xiong

- [High-resolution ac-pulse modulated electrohydrodynamic jet printing on highly insulating substrates](#)
Chuang Wei, Hantang Qin, Nakaira A Ramirez-Iglesias et al.

- [Comparing Modelling and Experiments for Prediction of Atmospheric Corrosion Under Controlled Dynamic Thin Film and Droplet Electrolytes](#)
Herman Albert Terry, Nils Van Den Steen, Keer Zhang et al.



ECS
The
Electrochemical
Society
Advancing solid state &
electrochemical science & technology

DISCOVER
how sustainability
intersects with
electrochemistry & solid
state science research

High frequency pulsed electrohydrodynamic printing with controllable fine droplets

Xin Yuan¹ and Zhenhua Xiong¹

State Key Laboratory of Mechanical System and Vibration, School of Mechanical Engineering, Shanghai Jiao Tong University, Shanghai 200240, People's Republic of China

E-mail: mexiong@sjtu.edu.cn

Received 9 March 2018, revised 1 May 2018

Accepted for publication 15 May 2018

Published 4 June 2018



CrossMark

Abstract

Most electrohydrodynamic printing technologies make it difficult to achieve controllable small droplets and high printing frequency simultaneously. In this paper, we investigate the influence of voltage, nozzle diameter and conductivity on printing frequency and droplet size, and introduce a parameter control method for achieving controllable fine droplets with high efficiency. The maximal printing frequency f_{pmax} of about 3.5 kHz with the smallest printed droplets diameter of about 16 μm can be achieved simultaneously via a normal size nozzle (ID 160 μm). Results show that the maximal printing frequency f_{pmax} can be enhanced by choosing large flow rate with medium duty cycle, such as 180 nl min^{-1} –50%, and can be increased with a larger voltage value and smaller nozzle. The study also reveals that droplet size steadily decreases with increased f_v and decreased nozzle diameter for large flow rate—duty cycle parameter group (180 nl min^{-1} –50%). Furthermore, under high frequency voltage, a lower voltage (1.8 kV) helps large-sized nozzles (30 G) generate smaller droplets. Droplet diameter control equations based on parameter adjustment are proposed. Droplet size accuracy and the effectiveness of parameter control are verified by analyzing actual dot matrix printing.

Keywords: electrohydrodynamic, printing, fine droplets, high frequency

(Some figures may appear in colour only in the online journal)

Nomenclature

ρ	Density of work liquid	ϵ_0	Permittivity of vacuum
σ	Surface tension	L	Characteristic length of ejected jet
K	Conductivity	d_j	Jet diameter
β	Relative dielectric constant	Ca	Capillary number
μ	Viscosity	Re	Reynolds number
$D(ID)$	Inner diameter of nozzle	Be	Electric bond number
OD	Outer diameter of nozzle	E_n	Electric field strength on meniscus
f_v	Voltage frequency	E_j	Electric field strength on jet
k_v	Voltage duty cycle	R	Radius of curvature
V_a	Peak voltage for DOD method	F_e	Electric field force
V_b	Basis voltage for DOD method	t_e	Voltage pulse width
V_a	Peak voltage for our method	τ_e	Charge relaxation time
t_{for}	Deformation time in one pulse	V_m	Static meniscus volume
t_p	Emission time in one pulse	ΔV	Dynamic meniscus volume
Q	Flow rate	f_{pmax}	Maximal printing frequency
f_p	Printing frequency	d_d	Printed droplet diameter
		f	Intercept of droplet diameter estimation equation
		S_d	Spacing between adjacent droplets
		U_x	Velocity of moving stage in x direction

¹ Author to whom any correspondence should be addressed.

1. Introduction

Many research fields need fine droplet generation, such as drug delivery, electronics, biochips and so on [1–3]. Inkjet printing technology—a conventional method to generate fine droplets—has the advantages of high positional precision, masklessness and being environmentally friendly [4–6]. However, it suffers from several drawbacks: the nozzle device is complicated and easily blocked by various liquids. Furthermore, the maximal ratio between nozzle diameter and droplet diameter is close to 1.89. To meet the fine droplet demand, inkjet nozzles must be very small, thus creating difficulty in nozzle fabrication.

Electrohydrodynamic printing (EHDP) is an alternative fine droplet generation technology developed in recent years, which makes droplet diameter range from hundreds of micrometers to hundreds of nanometers [7–9]. EHDP uses an electric field as the excitation source to stretch and break the liquid jet emitted from the tip of a nozzle to form small droplets. Printing results contain two major concerns, printing frequency and droplet size, which are affected not only by liquid properties, but also by external parameters, such as voltage frequency, flow rate and so on [9–11].

Considering printing frequency, Park *et al* used a nozzle of extremely small size to produce fine droplets with the diameter of about $2\mu\text{m}$ – $3\mu\text{m}$, at a printing frequency of 1 Hz [12]. The printing frequency of several other works is also 1 Hz [13–15], and has been enhanced to about 60 Hz by selecting appropriate parameters and liquids or using composite technologies [16–18]. Mishra and Kang enhanced the printing frequency to about 1 kHz by using special high voltage modulation and high conductivity liquid [19, 20].

As for droplet size, the ratio between nozzle diameter and droplet diameter can be used to evaluate the printing ability of different methods. Park *et al* printed droplets with the diameter of about $4\mu\text{m}$ – $8\mu\text{m}$ using nozzles with the inner diameter of $0.3\mu\text{m}$ – $2\mu\text{m}$ [12]. Shigeta *et al* printed small droplets with the diameter of about $4.5\mu\text{m}$ using nozzles of $0.5\mu\text{m}$ – $5\mu\text{m}$ [21]. Many research works have shown that the diameter of printed droplets is larger than the nozzle size [15, 22, 23]. Furthermore, based on several works [8, 20, 24–27], regardless of the nozzle diameter being less than $20\mu\text{m}$ or as large as $340\mu\text{m}$, the nozzle-to-droplet ratio is up to 4. Although this value is larger than the 1/1.89 of inkjet technology, it is still a challenging task to achieve large nozzle-to-droplet ratios.

Pulsed electrohydrodynamic (EHD) printing is a technique using meniscus self-oscillation excited by electric fields, which can provide both high emission frequency and extremely small ejected volume. Jurashek *et al* first found the useful high frequency mode in pulsed EHD printing [10]. Marginean *et al* discovered that printing frequency increases with nozzle radius in high frequency mode [28, 29]. Chen and Aksay found a relationship between printing frequency and the square of voltage [8]. Choi and Rogers believed that small flow rate could make emission frequency higher [24]. Other related works have mainly been concerned with the study of scaling law [30, 31]. However, there are few works

concerning the actual printing behavior or the control method of printing frequency and droplet size. In our previous work [32], small droplets with a maximal printing frequency of 500 Hz were achieved at voltage frequency of 20 Hz to 50 Hz. It is noted that there are multiple jet emissions during one voltage pulse, which makes droplet size hard to control and brings about instability in the printing process.

In this paper, we study the influence of the external parameters on printing frequency and droplet size in high frequency pulsed EHD printing. First, the single emission mode (one voltage pulse contains only one emission process) with higher efficiency and easier droplet size control is studied. Second, the relationship between maximal printing frequency and external parameters such as voltage, flow rate, nozzle size and conductivity is investigated. The relationship between droplet size and these external parameters is then also studied. Finally, parameter control equations of droplet diameter for achieving flexible fine droplet diameter with high printing frequency are proposed and verified.

2. Materials and experiment

2.1. Materials and key parameters selection

Ethylene glycol is chosen as the working liquid. To study the influence of conductivity, two additional ethylene glycol solutions respectively containing 1% and 2% sodium chloride are provided. Properties of pure ethylene glycol (named Gly1) are as follows: density $\rho = 1115\text{ kgm}^{-3}$, surface tension $\sigma = 48\text{ mNm}^{-1}$ (25°), conductivity $K = 1.07 \times 10^{-6}\text{ Sm}^{-1}$, relative dielectric constant $\beta = 38.66$ and viscosity $\mu = 16.9\text{ mPas}$ (25°). The two ethylene glycol solutions are named Gly2 and Gly3, and the conductivity values of these two solutions are $2.5 \times 10^{-6}\text{ Sm}^{-1}$ and $12.5 \times 10^{-6}\text{ Sm}^{-1}$; the other properties of Gly2 and Gly3 are very close to those of Gly1.

Four flow rates are used in this study; they are 1.5 nl min^{-1} , 18 nl min^{-1} , 54 nl min^{-1} and 180 nl min^{-1} . The voltage value ranges from 1.6 kV to 2.2 kV. Four sizes of nozzles are tested; they are 25 G (ID $250\mu\text{m}$, OD $460\mu\text{m}$), 30 G (ID $160\mu\text{m}$, OD $310\mu\text{m}$), 32 G (ID $110\mu\text{m}$, OD $250\mu\text{m}$) and 34 G (ID $60\mu\text{m}$, OD $200\mu\text{m}$).

2.2. Printing system

Figure 1 demonstrates the experimental setup of pulsed electrohydrodynamic printing. The printing system consists of four parts: a high voltage system, a liquid supply system, a spray system and a motion stage. The high voltage system is made up of a digital function generator and a high voltage amplifier (AFG 2000 Function Generator, TREK MODEL 10/10B-HS High Voltage Amplifier). The digital function generator produces a square wave with adjustable duty cycle and frequency, which will then be amplified by the voltage amplifier. In this paper, the applied voltage is fixed as 2.0 kV, while voltage frequency f_v and duty cycle k_v are tunable. The liquid supply system contains a syringe pump (Pump 11 ELITE Nanomite, HARVARD Inc) and an injector with the capacity

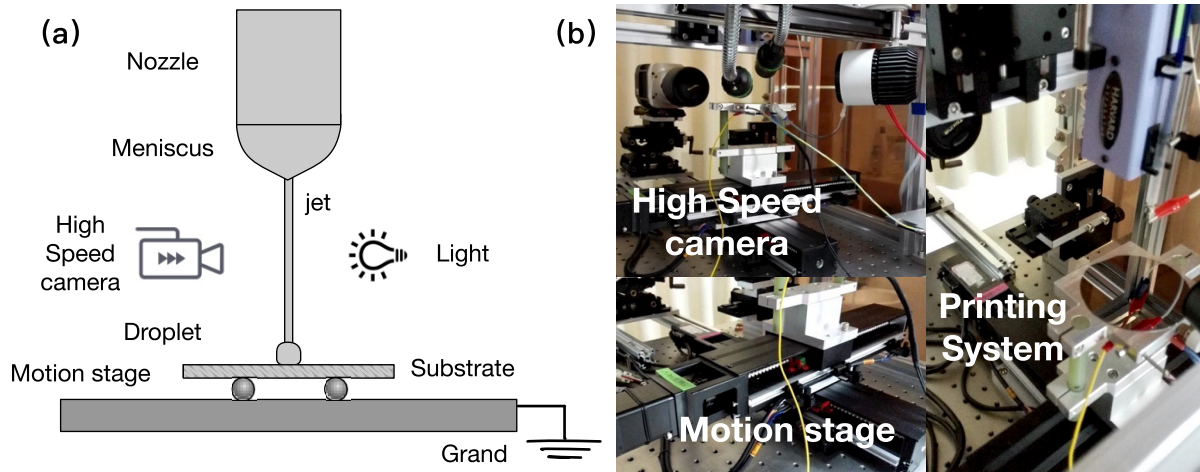


Figure 1. Experiment setup of the pulsed EHD printing system: (a) the schematic of setup; (b) the experimental system.

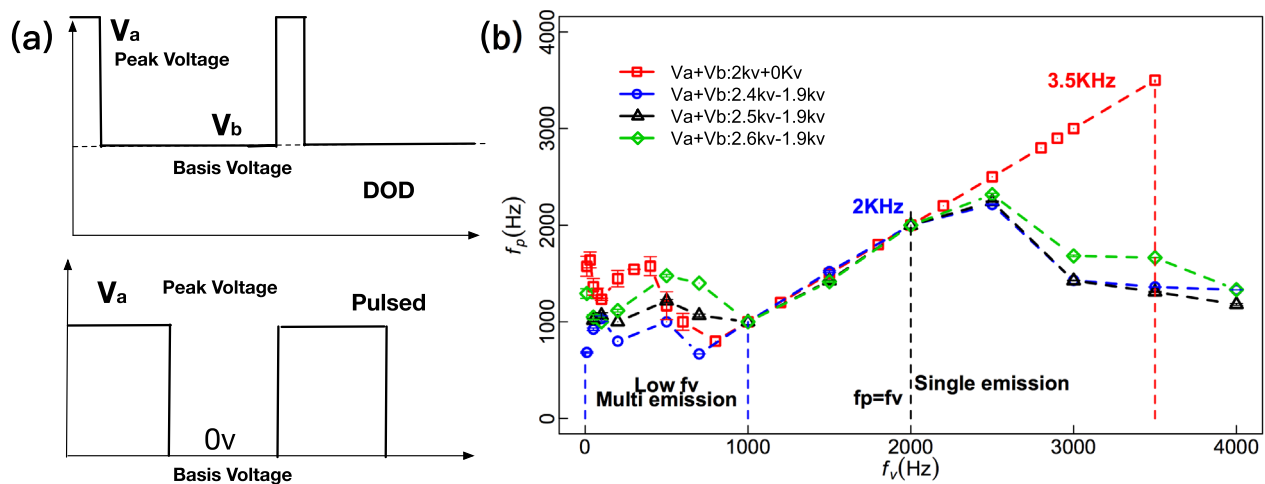


Figure 2. Voltage modulation and the presentation of printing frequency in DOD and pulsed EHD method. (a) Voltage modulation: V_a and V_0 are peak voltages in the two methods; V_b and 0V are both basis voltages. (b) Printing frequency: f_p changes with voltage frequency in both methods; nozzle 32 G, liquid is ethylene glycol, flow rate is 180 nl min^{-1} .

of 1 ml. The stainless steel disk with a hydrophobic surface is chosen as the substrate (contact angle is larger than 90°). The distance between nozzle and substrate is set as 1 mm.

The motion stage system is composed of two electrical motors and two linear guides (Mitsubishi Electronics HC-MF053 and HC-MF13, linear guides HI-WIN KK60). This X–Y motion stage has a repeated positioning accuracy of $3 \mu\text{m}$. Furthermore, detailed deformation behaviors can be observed by using a high speed camera (Phantom Micro M310, maximum frame rate ~ 650000 frames per second) fitted with a zoom lens (Navitar, 4–10 \times continuously adjustable zoom). The frame rate used in this paper is 10000 fps, and the resolution is set as 320×424 .

2.3. High frequency pulsed electrohydrodynamic printing process

When the voltage frequency is low, there are several jet emissions during one voltage pulse [32]. During one voltage pulse, the droplet size varies slightly, which brings difficulty in droplet size control. In order to enhance printing frequency

f_v , voltage frequency should be increased, and as a result, the number of emissions during one voltage pulse quickly reduces to 1. The emission behavior at low voltage frequency is thus named as multiple emission mode, while the lone emission in one voltage pulse printing mode is named as single emission mode. It can be seen later that single emission mode is more suitable for achieving high frequency printing results.

Figure 2 presents the voltage modulation and the printing frequency of printed droplets under the two emission modes. As shown in figure 2(a), V_a is the peak voltage and V_b is the basis voltage. Unlike the drop-on-demand EHD technique (DOD EHD), which imposes a high peak trigger voltage on the basis voltage to effect single droplet separation [20], we apply a voltage signal with large voltage difference and medium duty cycle in order to enable the meniscus to generate a stable stimulated self-oscillating micro-jet emission. Four voltage parameter groups are tested and shown in figure 2(b). For DOD EHD, V_b is set as 1.9kV, and V_a are 2.4kV, 2.5kV and 2.6kV. For pulsed EHD, V_a and V_b are 2kV and 0, which voltage difference is larger than that of DOD EHD (2kV to about 0.6kV). In figure 2(b), it can be seen that printing

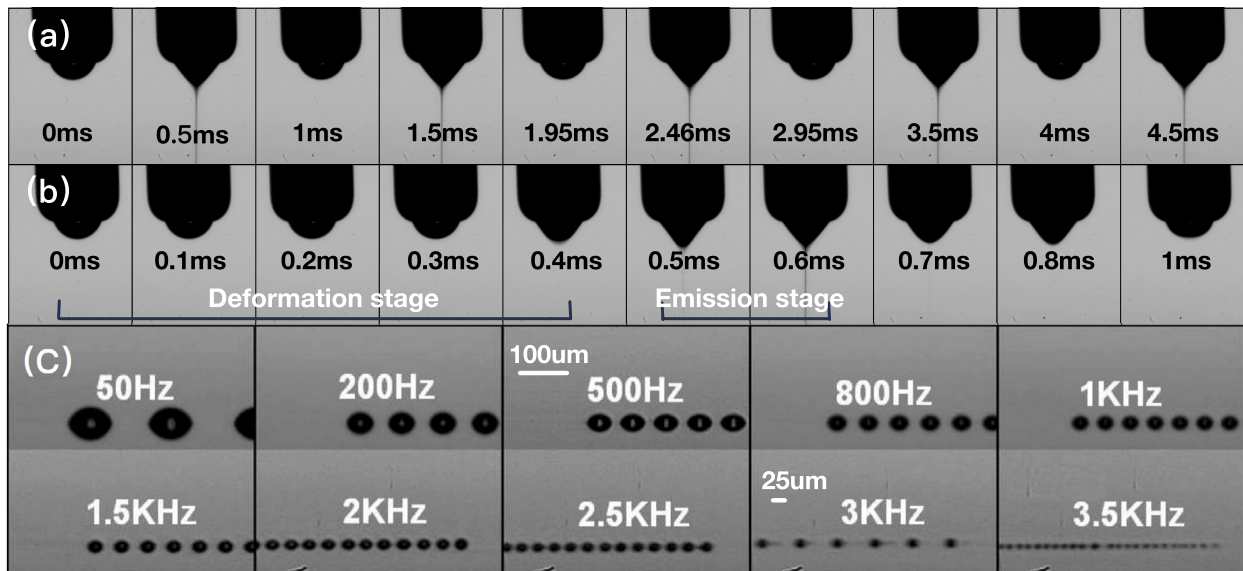


Figure 3. High speed images of high frequency emission behavior and the deposited droplets, voltage is 2kV, flow rate is 180 nl min^{-1} , and duty cycle k_v is 50%: (a) detailed behaviors of five successive emissions with time, nozzle 30 G, $f_v = 1 \text{ kHz}$; (b) detailed deformation behavior of the meniscus in one single emission, nozzle 30 G, $f_v = 1 \text{ kHz}$; (c) size of printed droplets change with voltage frequency f_v , nozzle 32 G.

frequency f_p under DOD method starts to decrease after voltage frequency f_v reaches 2.2kHz and deviates from f_v after 2kHz. Therefore, DOD EHD at high frequency voltage cannot guarantee that one voltage pulse contains only one emission at high f_v . However, the proposed voltage configuration always ensures that printing frequency f_p is equal to f_v even under high voltage frequency up to 3.5kHz, which can improve the control stability of high frequency pulsed EHD printing.

Figure 3 shows high speed images of printing behavior and deposited droplets via high frequency pulsed EHD. Figure 3(a) demonstrates five successive emissions under single emission mode. Every two adjoining emissions have a very close time interval of about 0.5 ms, which further proves that single emission mode can be used as a high frequency printing method. Figure 3(b) shows detailed deformation behavior of the meniscus over an entire emission process. Based on the change of meniscus shape [33], we can divide a single emission process into three stages: deformation stage, emission stage and recovery stage. t_{for} defines the time of deformation stage in a voltage pulse, from when the voltage is triggered until the tip of the meniscus is ready to eject the jet (shown in figure 3(b), from 0 ms to 0.4 ms). t_p defines the time of emission stage in a voltage pulse, from the jet beginning to eject at the tip of the meniscus to the end of the detachment between the jet and the meniscus (shown in figure 3(b), from 0.4 ms to 0.6 ms).

Taking into account that the high frequency printing behavior is significantly affected by meniscus morphological deformation and external parameters, the deformation stage and emission stage with two characteristic times t_{for} and t_p are particularly important. Higher printing frequency means shorter voltage pulse (larger f_v), so the deformation time t_{for} and emission time t_p also need to be reduced. Since characteristic

deformation time and emission time are strongly related to the meniscus deformation behavior and the electric field effect [8, 11, 24, 29, 30], we believe that flow rate Q (liquid pressure influences meniscus state), nozzle inner diameter D (which determines meniscus volume with Q) and duty cycle k_v (when voltage is constant, duty cycle decides electric field effect) are the key external parameters influencing the printing results.

3. Printing frequency study

In single emission mode, printing frequency f_p rises steadily with f_v until the meniscus cannot form an entire emission process with an extremely short voltage pulse. Meanwhile, printing frequency is also affected by nozzle diameter D , flow rate Q and duty cycle k_v . Because nozzle diameter directly influences meniscus volume, which in turn determines other parameters, we fix nozzle size as a constant in this study, and mainly focus on the relationships between printing frequency and external parameters Q and k_v .

3.1. Printing frequency f_p changes with flow rate and duty cycle $Q - k_v$

Figure 4 shows how f_p changes with f_v under various flow rate–duty cycle configurations. As shown in figure 4, from low voltage frequency to high frequency, f_p in multiple emission mode may reach up to 500 Hz, and the printing frequency f_p varies a lot between different $Q - k_v$ configurations. When f_v is generally larger than 500Hz, the pulsed printing under a given $Q - k_v$ group turns into single emission mode, where the two frequencies are equal $f_p = f_v$. Compared with printing frequency at small flow rate (1.5 nl min^{-1} in figure 4(a) and 18 nl min^{-1} in figure 4(b)), it is shown that printing frequency can increase from 1 kHz to about 3.5kHz for the

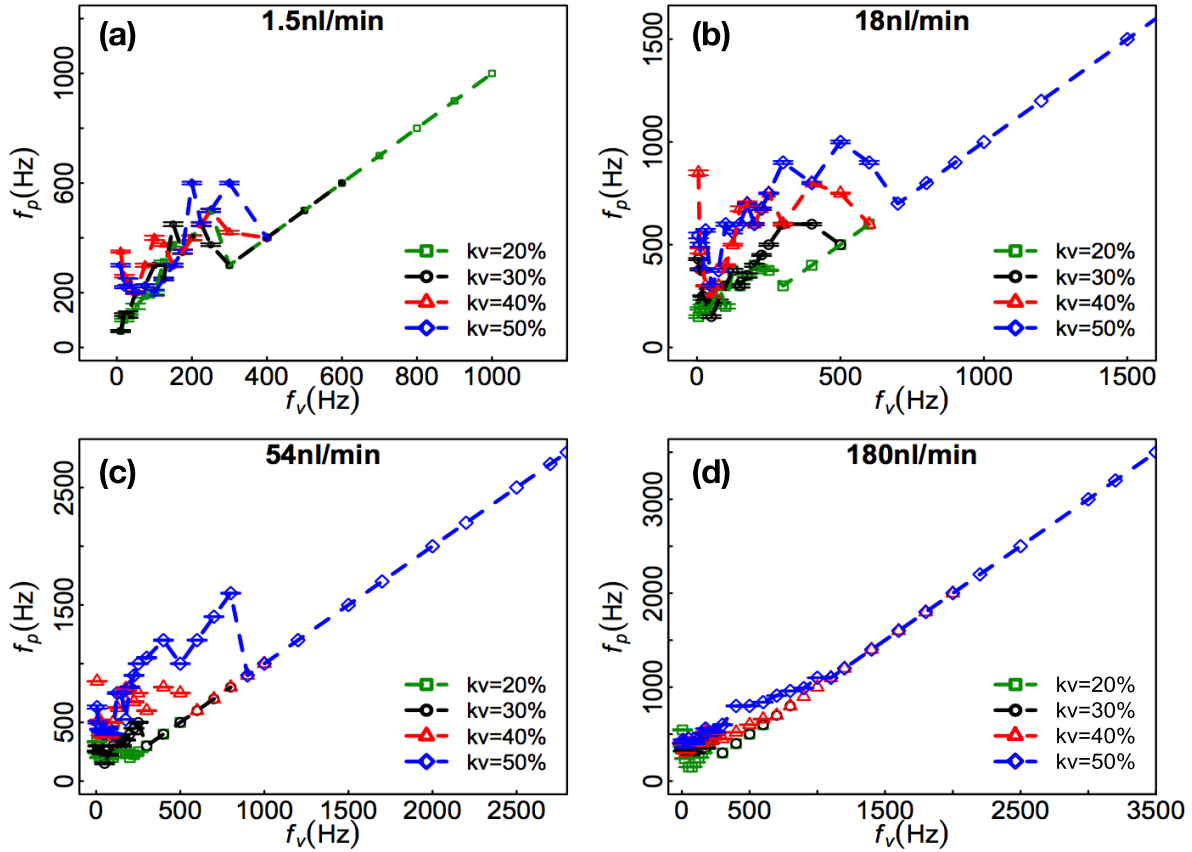


Figure 4. Printing frequency f_p changes with f_v under different $Q - k_v$ groups. Duty cycle values k_v are 20%, 30%, 40% and 50%. Voltage is 2 kV, nozzle 30 G: (a) $Q = 1.5 \text{ nl min}^{-1}$; (b) $Q = 18 \text{ nl min}^{-1}$; (c) $Q = 54 \text{ nl min}^{-1}$; (d) $Q = 180 \text{ nl min}^{-1}$.

large flow rate and duty cycle group (180 nl min^{-1} –50% in figure 4(d)). Meanwhile, at the flow rate of 1.5 nl min^{-1} in figure 4(a), a printing frequency of 1 kHz can also be obtained by choosing a small flow rate and duty cycle group (1.5 nl min^{-1} –20% and 1.5 nl min^{-1} –30%). Thus, large $Q - k_v$ (180 nl min^{-1} –50%) and small $Q - k_v$ (1.5 nl min^{-1} –20% or 30%) configurations are both beneficial to high frequency printing behavior.

This effect—in which two kinds of $Q - k_v$ groups are both helpful for getting high printing frequency—can be explained as follows. According to Calvos’ studies [11, 34], surface tension, inertial force and viscous force are the main forces that hinder meniscus deformation, as is shown in equation (1) (d_j is the jet diameter, L is the characteristic length of ejected jet):

$$\{\sigma d_j^{-1} L^{-1}, \rho Q^2 d_j^{-4} L^{-1}, \mu Q d_j^{-2} L^{-2}\} \quad (1)$$

$$\begin{cases} Ca = \mu \frac{4Q}{\pi D^2 \sigma} \\ Re = \frac{4\rho Q}{\mu D \pi} \\ Be_{,cone} = \frac{\epsilon_0 E_n^2 R}{2\sigma} \\ Be_{,jet} = \frac{\epsilon_0 E_j^2 d_j}{4\sigma}. \end{cases} \quad (2)$$

Therefore, the magnitudes of various forces can be compared in terms of the capillary number Ca , Reynolds number Re and electric Bond number Be . Referring to [35, 36], Ca , Re and Be can be calculated by equation (2). Among them, $Be_{,cone}$ and $Be_{,jet}$ are the electric bond numbers of the meniscus and

the jet, which are used to compare the magnitude of the electric field force and the surface tension. Ca is related to flow rate–nozzle combination, but no matter how flow rate and nozzle size change, the maximal Ca is 0.0015, much smaller than 1, which means that the viscous force is negligible compared with surface tension [37]. Similarly, Re has a maximal value of 0.0042 (much less than 1) for different flow rate–nozzle combinations, which means that inertial force is negligible compared to surface tension. According to COMSOL simulation, E_n and E_j are $3.4 \times 10^6 \text{ Vm}^{-1}$ and $2.2 \times 10^7 \text{ Vm}^{-1}$ respectively. R and d_j are set to $80 \text{ }\mu\text{m}$ and $10 \text{ }\mu\text{m}$ (Nozzle 30 G). Thus, $Be_{,cone}$ and $Be_{,jet}$ are 0.4 and 7.67. This shows that electric field force and surface tension on the meniscus are of the same order of magnitude, and the two forces influence each other to determine the jet emission behavior:

$$\begin{cases} V_m = \frac{\pi D^3}{24 \tan \theta} \\ \Delta V = \frac{Q(1-k_v)}{f_v}. \end{cases} \quad (3)$$

Let us focus on the specific performance of electric force and surface tension with variation of parameter values. For k_v in $Q - k_v$, at the same f_v , a small k_v (20%) means short t_e and small impulse momentum $F_e t_e$ ($F_e = 1/2 \beta \epsilon_0 E_n^2$), indicating that the electric effect enhances with increased k_v because of t_e . For Q in $Q - k_v$, when meniscus enters the no-E field period ($(1 - k_v)/f_v$), the meniscus volume changes with flow rate Q . According to our previous research [32], it can be seen that the static meniscus volume V_m (voltage not triggered) and

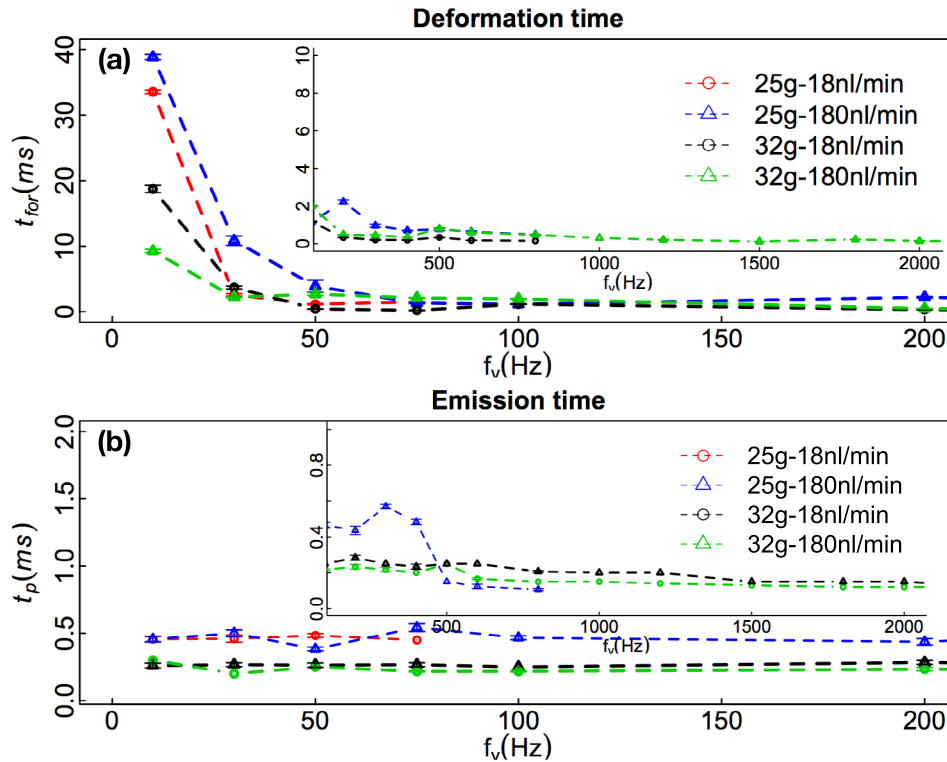


Figure 5. Deformation time t_{for} and emission time t_p change with Q and D , voltage is 2kV, duty cycle is 50%, nozzles are 25 G and 32 G, flow rates are 18 nl min⁻¹ and 180 nl min⁻¹: (a) t_{for} ; (b) t_p .

the dynamic meniscus volume ΔV (volume increment within no-E field period) can be calculated with equation (3) (θ is the Taylor cone angle). V_m does not change with flow rate, it is $2.82 \times 10^{-16} \text{ m}^3$ – $5.36 \times 10^{-13} \text{ m}^3$ (34 G to 30 G). ΔV varies with Q and f_v . Comparing ΔV at 1.5 nl min⁻¹ and 180 nl min⁻¹ (set $k_v = 50\%$ and f_v ranges from 50 Hz to 2kHz), it can be seen that ΔV at large Q is close to V_m (ΔV range: $7.5 \times 10^{-16} \text{ m}^3$ – $3 \times 10^{-14} \text{ m}^3$), which clearly increases the radius of curvature R , thereby increasing the surface tension.

Therefore, when $Q - k_v$ is small (1.5 nl min⁻¹–20%), both electric field effect and surface tension are weak, so that printing behavior is stable and the f_p is large (1 kHz) because of the balance. Similarly, when $Q - k_v$ is large (180 nl min⁻¹–50%), large electric field intensity with large surface tension can generate oscillation behavior with large amplitude, further improving the printing stability and enhancing the maximum of f_p .

Compared to the small $Q - k_v$ group, the maximal printing frequency f_{pmax} (which is defined to compare the print ability of different parameter configurations) at large $Q - k_v$ increases from 1 kHz to 3.5 kHz. This is because large flow rate brings greater resistance, and larger duty cycle makes t_e larger. The interaction between these two forces (according to equation (2)) has a greater impact on the meniscus, resulting in shorter characteristic deformation time and emission time. Figure 5 shows the variation of characteristic time t_{for} and t_p for various flow rates and nozzle sizes. When the nozzle is 32 G, t_{for} of 180 nl min⁻¹ is obviously less than that of 18 nl min⁻¹ under low voltage frequency, and is even slightly smaller under high voltage frequency. Similarly, t_p of 180 nl min⁻¹ is also slightly less than that of 18 nl min⁻¹. In addition,

we also found that nozzle diameter also significantly affects characteristic time. According to Poiseuille’s law, the larger the nozzle diameter is, the smaller the liquid pressure and the impaction are. So t_{for} and t_p are both larger for large nozzles than for small nozzles. Furthermore, when nozzle is 25 G, t_{for} of 180 nl min⁻¹ is larger than that of 18 nl min⁻¹. This is probably because the volume of meniscus of 25 G is much larger than that of 32 G and the increased volume during the period of no electric field under low voltage frequency will be integrated into the meniscus and prevent the meniscus deformation instead of impacting the meniscus to reduce characteristic time. Thus, the large $Q - k_v$ group is useful for achieving high printing frequency.

It is possible to increase the printing frequency by further increasing the duty cycle. Figure 6 shows how the printing frequency varies with duty cycle. The flow rate is 180 nl min⁻¹, and the duty cycle increases from 50% to 90%. As shown in figure 6, when duty cycle are 50% and 60%, maximal printing frequency f_{pmax} are both 3.5 kHz. When duty cycle is 80%, f_{pmax} is 3 kHz. When duty cycle reaches 90%, f_{pmax} is quickly reduced to 700 Hz. In summary, for high frequency pulsed EHD printing, large flow rate with moderate duty cycle, such as 180 nl min⁻¹–50% or 60%, can enhance the maximal printing frequency f_{pmax} .

3.2. Maximal printing frequency f_{pmax}

In high frequency pulsed EHD printing, maximal frequency f_{pmax} reflects the influence of parameter selection on printing frequency. The previous analysis shows that nozzle diameter changes printing frequency by affecting the characteristic

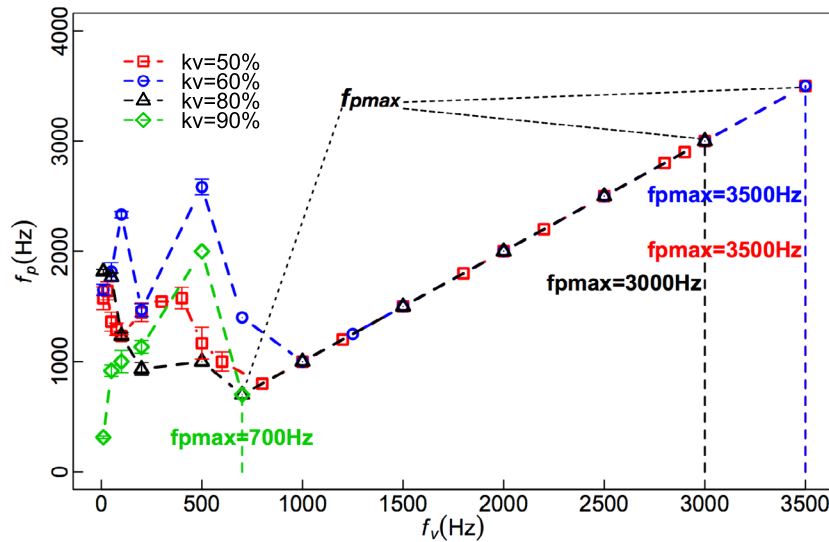


Figure 6. Printing frequency f_p changes with duty cycle k_v . Flow rate Q is 180 nl min^{-1} , nozzle is 30 G, voltage is 2 kV.

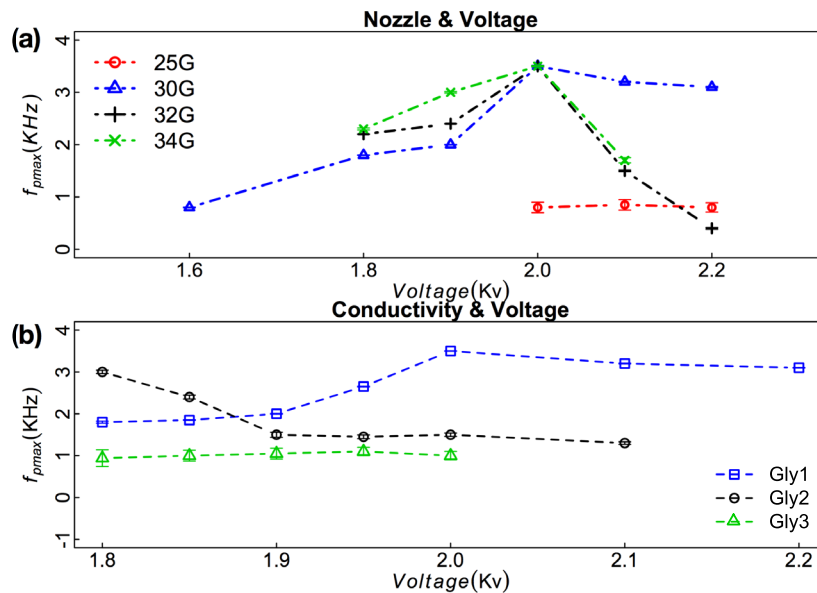


Figure 7. Maximal printing frequency f_{pmax} changes with nozzle size, voltage value and conductivity: (a) f_{pmax} changes with voltage and nozzle size, flow rate is 180 nl min^{-1} , voltage ranges from 1.6 kV to 2.2 kV, nozzles are 25 G, 30 G, 32 G and 34 G; (b) f_{pmax} changes with conductivity, flow rate is 180 nl min^{-1} , nozzle is 30 G. Conductivity of three ethylene glycol solutions is $1.07 \times 10^{-6} \text{ Sm}^{-1}$, $2.5 \times 10^{-6} \text{ Sm}^{-1}$ and $12.5 \times 10^{-6} \text{ Sm}^{-1}$.

times of meniscus, and that the voltage amplitude also influences printing frequency by affecting electric field force [24, 32]. Figure 7(a) demonstrates that f_{pmax} changes with nozzle diameter and voltage.

In figure 7(a), with a large nozzle (25 G), f_{pmax} is close to 1 kHz and barely changes with voltage. This is because the static meniscus volume V_m under nozzle 25 G is quite large (hundreds times the meniscus volume of nozzle 30 G and smaller nozzles), larger inertial force makes it difficult for the voltage increment of 0.2 kV (2 kV to 2.2 kV) to enhance the degree of meniscus deformation significantly and result in smaller characteristic time to cause larger f_{pmax} . With the other three nozzles (30 G, 32 G and 34 G), f_{pmax} increases with voltage when it is lower than 2 kV. Compared with the case of

25 G, smaller V_m values (smaller nozzles) are beneficial for causing greater tensile effect, which results in rapid deformation and larger f_{pmax} . Therefore, choosing a small nozzle (34 G) and large flow rate (180 nl min^{-1}), f_{pmax} can reach 3 kHz to 3.5 kHz when voltage rises up to 2 kV.

We also observed that as the nozzle diameter decreases, the effective voltage range of f_{pmax} (voltage range can ensure the probable increase of f_{pmax} with voltage) decreases. For example, the effective voltage range is 1.6 kV to 2.2 kV under nozzle 30 G, while it is only 1.8 kV to 2 kV under nozzles 32 G and 34 G. This shows that larger nozzle size helps to achieve a more stable and wider effective voltage range for f_{pmax} . Meanwhile, when voltage is larger than 2 kV, f_{pmax} of 32 G and 34 G decreases rapidly to about 1 kHz at 2.1 kV.

At 2.2 kV, high frequency emission behavior cannot be established with nozzle 34 G. This is because a small nozzle with small meniscus makes deformation behavior sensitive to voltage change, which easily leads to printing interruption under large voltages. In summary, a small nozzle with a rather large voltage, such as 34 G–2 kV, can get a large f_{pmax} (3.5 kHz). Meanwhile, by selecting a moderate nozzle, such as 30 G, with a large flow rate and voltage (such as 180 nl min⁻¹–2 kV), we can get a stable high frequency printing process with large f_{pmax} over a wide effective voltage range (1.6 kV to 2.2 kV).

According to previous studies [38, 39], large conductivity can significantly improve liquid reaction rate to the electric field. Figure 7(b) shows the change of f_{pmax} with voltage frequency for three liquids of different conductivity. When conductivity is low (Gly1), f_{pmax} increases with voltage, the overall upward trend is stable and the error is small. With Gly2, f_{pmax} can reach 3 kHz at 1.8 kV, and it starts to fall and remains stable at about 1.5 kHz when voltage rises. With large conductivity of Gly3, f_{pmax} always stays around 1 kHz, not affected by the increase of voltage.

As is well known, conductivity affects charge transport rate on meniscus, and causes differences in charge relaxation time $\tau_e = \beta\epsilon_0/K$. τ_e of Gly1 is 0.314 ms, τ_e of Gly2 and Gly3 are 0.134 ms and 0.027 ms. At the same time, fluid movement also affects meniscus deformation, which leads to the influence of f_{pmax} . Thus, fluid characteristic time t_l calculated by $\pi d_f^2 L/Q$ (L is close to 0.7 mm, Q is set as 180 nl min⁻¹) is given [32, 40]. However, the fluid speed calculated from t_l is 0.04 m s⁻¹, and the jet speed calculated from high speed image and emission time t_p (based on figure 5(b)) is 7 m s⁻¹. This shows that the key factor determining the smallest characteristic times t_{for} and t_p is the electric response time rather than fluid movement. This is consistent with the previous analysis of the magnitude of multiple forces. Thus, the charge relaxation time τ_e determines the response time of the system—that is, the value of f_{pmax} .

Low conductivity and large τ_e (Gly1) are more conducive to the establishment of oscillation–stretching mechanisms under high frequency voltage ($f_v > 2$ kHz), making the high frequency emission behavior of the meniscus more persistent and stable for generating jets. As τ_e decreases with increased conductivity, although the deformation rate increases (t_{for} and t_p decreases slightly), the emission behavior becomes unstable, results in maximal f_{pmax} of Gly2 and Gly3 less than 2 kHz. In addition, when voltage is small (1.8 kV), Gly2 with smaller τ_e is more likely to obtain a high f_{pmax} , while Gly3 has relatively large conductivity, which causes the meniscus to be too easily broken up under small f_v ($f_{pmax} = 0$ at voltage greater than 2 kV) [35].

In summary, f_{pmax} increases with increased voltage and decreased nozzle size. A nozzle with moderate size (Nozzle 30 G) is more conducive to a stable and efficient printing result (large f_{pmax} and large effective voltage range: $f_{pmax} = 3.5$ kHz, voltage range is 1.6 kV to 2.2 kV). In addition, relatively small conductivity is conducive to the establishment of a stable oscillation emission mechanism under high frequency voltage, which leads to a large f_{pmax} of 3.5 kHz.

4. Droplet size study

Many researchers agree that emission time t_p only changes with conductivity and determines the amount of ejected jet [10, 32, 33]. However, after testing on several different $Q - k_v$ groups, we found that t_p also decreases slightly with increased f_v . t_p reduces from the early 0.4 ms–1 ms to about 0.1 ms–0.2 ms at very high voltage frequency (above 3 kHz). This means that meniscus shape in high frequency pulsed EHD printing varies with the external parameters. Because the meniscus morphological variations are influenced by the meniscus initial volume (mainly decided by nozzle size) and the flow in nozzle (affected by flow rate) during the electric field period, the flow rate, nozzle diameter, voltage and conductivity all need to be considered when droplet size is studied. Here, we focus on droplet diameter changes in single emission mode, which means that voltage frequency f_v is at least 500 Hz.

4.1. Droplet diameter d_d changes with nozzle diameter D

Figure 8 shows that droplet diameter d_d changes with nozzle diameter and flow rate. The figure clearly reveals that, no matter how big the nozzle is, droplet diameter at large flow rates (54 nl min⁻¹ to 180 nl min⁻¹) decreases steadily with increasing voltage frequency. However, when flow rate Q is as small as 18 nl min⁻¹, the decreasing rate of droplet diameter d_d is a little bit higher, especially for the nozzle 34 G. With this nozzle, d_d decreases to less than 10 μ m when f_v reaches 1.8 kHz (the smallest droplets with the diameter of about 8 μ m can be achieved at 180 nl min⁻¹–34 G). This is because the 34 G nozzle, whose meniscus volume is only 1/20 of that of the 30 G nozzle (the cube of the ratio between the two inner diameters = (60/160)^{1/3}), has a small meniscus that is more sensitive to voltage. Hence, droplet diameter reduces even faster for a small nozzle with small flow rate (18 nl min⁻¹–34 G).

Considering that large flow rate contributes to stable high frequency pulsed EHD printing, we investigated droplet diameter control mainly at the flow rate of 180 nl min⁻¹ and the duty cycle of 50%. Figure 9(a) shows the relationship between d_d and f_v with four different nozzles. For nozzle 25 G, meniscus volume is too large to eject jets at high voltage frequency. When the nozzle is changed from 30 G to 34 G, d_d decreases under the same f_v . To get controllable fine droplets, a small nozzle with large flow rate should be chosen.

4.2. Droplet diameter d_d changes with voltage

Figure 10 demonstrates the effect of voltage on droplet size under different nozzle–flow rate configurations. As mentioned before, when $Q - k_v$ is 180 nl min⁻¹–50%, more stable emission behavior under high frequency voltage can be obtained. Therefore, in figure 10(a), we choose to fix 180 nl min⁻¹–50%, and check the $d_d \sim f_v$ relationship for three nozzles (30 G, 32 G and 34 G). With nozzle 30 G, when voltage is 1.8 kV, d_d rapidly decreases with an increase of f_v . When

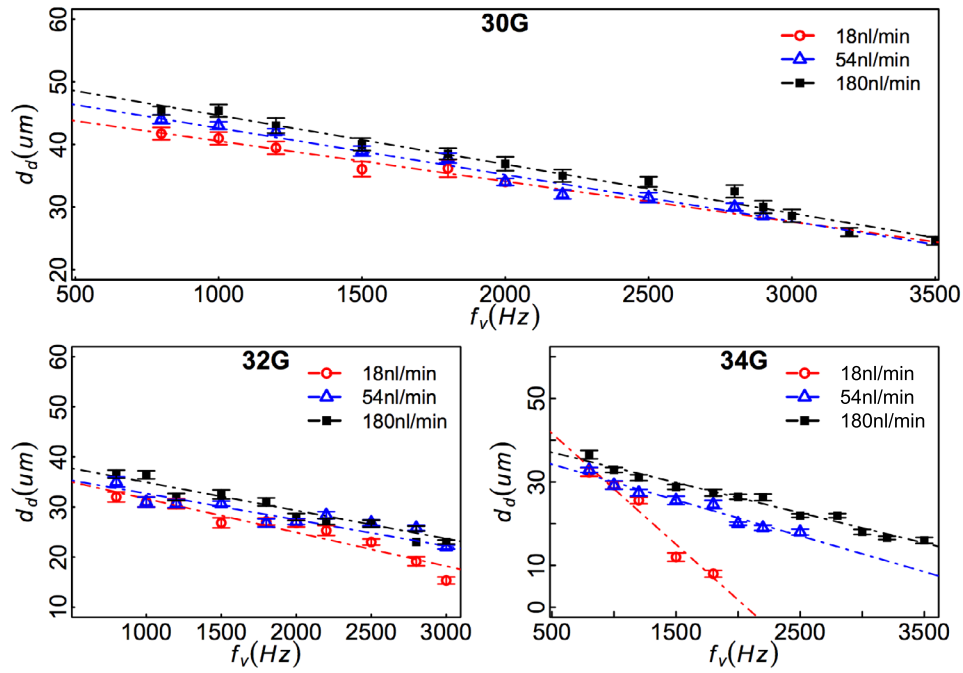


Figure 8. Droplet diameter d_d changes with nozzle diameter and flow rate. Voltage is 2 kV, duty cycle is 50%. Three nozzles are 30 G, 32 G and 34 G. Three flow rates are 18 nl min^{-1} , 54 nl min^{-1} and 180 nl min^{-1} .

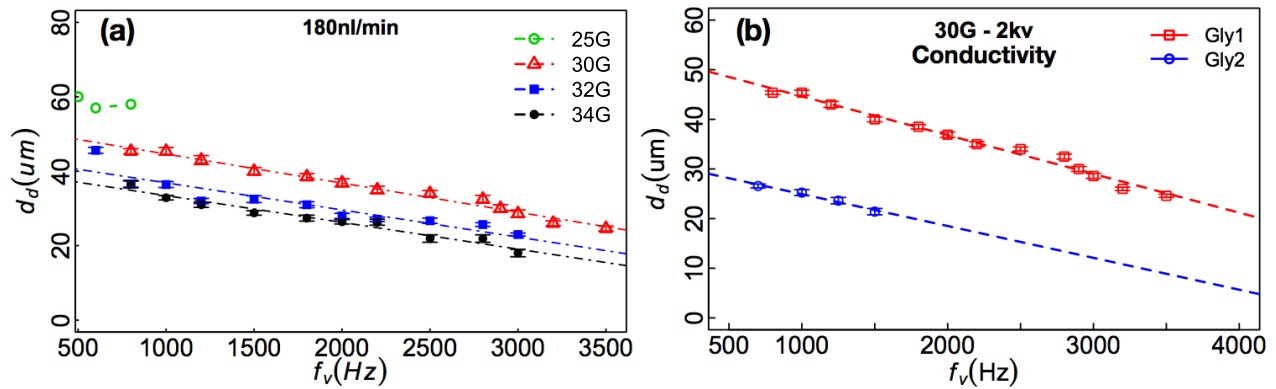


Figure 9. Relationship between d_d and f_v with various nozzles and liquid conductivities. Voltage is 2 kV, duty cycle is 50%: (a) four nozzles are tested with Gly1 liquid; (b) nozzle 30 G, Gly1 and Gly2 are tested. Conductivity of Gly2 is larger than that of Gly1.

voltage is up to 2 kV, d_d decreases slowly, and it is smaller at 1.8 kV than that at 2 kV under a high frequency voltage ($f_v > 1\text{kHz}$). With nozzle 32 G, the smaller meniscus volume V_m makes the meniscus more easily deformed and broken at low voltage, so the voltage increase has little effect on d_d . Similarly, the d_d of 1.8 kV at high frequency voltage is smaller than that of 2 kV, and the transition voltage frequency rises from 1.2 kHz at 30 G to 3 kHz at 32 G. With nozzle 34 G, the V_m of 34 G is 1/8 that of 32 G and 1/20 that of 30 G. A smaller meniscus is more sensitive to voltage change, and the droplet is smaller when the voltage is 1.8 kV. This is because, at 2 kV, an excessively small meniscus enhances the stretching effect of the electric field, making the oscillation amplitude too large; the volume of ejected jet increases, and the printed droplet size increases too.

Figure 10(c) shows the slope of the fit curves in figure 10(a). For a large voltage, such as 2 kV, the change in nozzle size has almost no effect on the $d_d \sim f_v$ relationship. For smaller

voltages, such as 1.8 kV, d_d quickly decreases with larger nozzles (e.g. 30 G), but slowly decreases with smaller nozzles (e.g. 34 G). Furthermore, considering that small droplets can also be formed at small flow rates, we tried to study the effect of voltage change on droplet size at 18 nl min^{-1} (seen in figure 10(b)). Obviously, it can be seen that d_d barely changes when voltage rises from 1.8 kV to 2 kV, indicating that droplet size is not sensitive to voltage changes for small flow rates with large nozzles (18 nl min^{-1} –30 G).

Referring to the flow focusing phenomenon of the study [36, 41], droplet diameter increases with voltage. Here, under high frequency voltage, the meniscus of a low conductivity liquid is more likely to exhibit high frequency oscillation behavior. At high frequency voltage, a small voltage (1.8 kV) tends to cause the tip of the meniscus to eject jets and form small droplets, while larger voltage (2 kV) tends to generate large droplets because of the overall oscillation of the meniscus. For example, the smallest droplet can be obtained

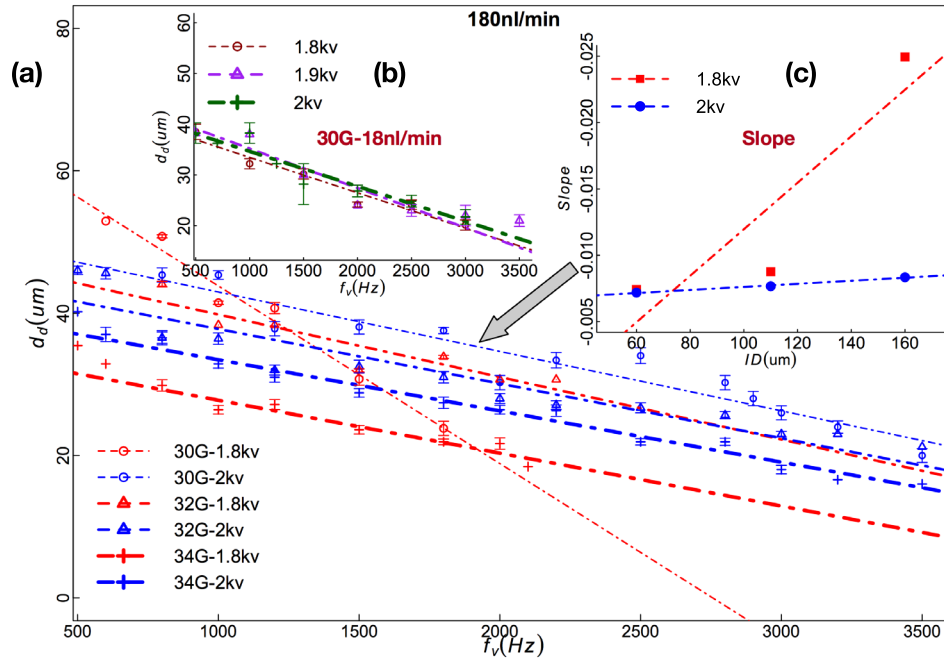


Figure 10. Droplet diameter d_d changes with f_v under different nozzle size and voltage: (a) flow rate is 180 nl min^{-1} and nozzles are 30 G, 32 G and 34 G. Voltage is 1.8 kV to 2 kV, and k_v is 50%. (b) $d_d \sim f_v$ under small flow rate of 18 nl min^{-1} with nozzle 30 G (c) slope of $d_d \sim f_v$ fitting curves under 180 nl min^{-1} ; other parameters are the same as in (a).

by choosing 34 G–1.8 kV with 180 nl min^{-1} . However, 2 kV is more suitable to the development of a stable and controllable printing process with large f_{pmax} and effective voltage range, referring to the analysis of f_{pmax} .

4.3. Droplet diameter control equation

According to figures 8 and 9, regardless of the change in nozzle diameter or conductivity, the slope of the relationship between droplet diameter d_d and f_v at 180 nl min^{-1} is relatively stable, which helps us to establish the control equation of droplet diameter. We selected nozzle 34 G to establish these fitting equations (30 G and 32 G can also be chosen to establish equations according to figure 9(a)). The flow rates of 18 nl min^{-1} and 180 nl min^{-1} are both considered, for obtaining extremely small printed droplets and fine droplets with higher printing frequency respectively. Equation (4) and (5) are droplet diameter control equations at 18 nl min^{-1} and 180 nl min^{-1} respectively.

Based on the analysis of droplet diameter above, we believed that the small nozzle, large $Q - k_v$ group as 180 nl min^{-1} –50% with appropriate voltage value (2 kV in this study) should be chosen for achieving controllable fine droplets with high printing frequency:

$$d_d = -0.0266f_v + 55 \tag{4}$$

$$d_d = -0.0072f_v + f \tag{5}$$

$$\frac{f_1}{f_2} = \left(\frac{OD_1}{OD_2}\right)^{1/3}. \tag{6}$$

f is the intercept of equation (5) at 180 nl min^{-1} , and is equal to 40.64. Besides, based on the variation of droplet diameter under different nozzles (as seen in figure 9(a)), the

relationship between the intercept f and the nozzle outer diameter OD for equation (5) is revealed in equation (6). With the help of these equations, we can use nozzle 34 G ($ID 60 \mu\text{m}$) to print droplets with the minimal diameter of about $8 \mu\text{m}$ – $10 \mu\text{m}$. Similarly, we can print droplets with the minimal diameter of about $16 \mu\text{m}$ – $18 \mu\text{m}$ by using nozzle 30 G ($ID 160 \mu\text{m}$). The printing frequency of these fine droplets ranges from 1.5 kHz to 3 kHz or even higher, which guarantees printing efficiency.

5. Printing results verification

To verify the high frequency pulsed EHD printing with droplet diameter control, different patterns of fine droplets are demonstrated in this section.

Figure 10 shows the actual printing results of droplets with four different diameters. The diameter of droplets in figure 11(a) is $35 \mu\text{m}$, the diameter in figure 11(b) is $24 \mu\text{m}$, and the diameters in figure 11(c) are $18 \mu\text{m}$ and $14 \mu\text{m}$ respectively. Droplets with $14 \mu\text{m}$ diameter are printed at 34 G– 18 nl min^{-1} , the printing frequency f_p is 1.35 kHz. The other three sizes of droplets are printed at 34 G– 180 nl min^{-1} .

Here is the high frequency pulsed EHD printing process. Focused on those droplets printed at 180 nl min^{-1} , we first determine the desired droplet diameter, such as $35 \mu\text{m}$, $24 \mu\text{m}$ and $18 \mu\text{m}$. We then estimate the approximate printing frequency f_p according to equation (4). Based on these equations, the three calculated printing frequencies are 783 Hz, 2.3 kHz and 3.15 kHz. Next, fixing other parameters and referring to estimated printing frequencies, we adjust the voltage frequency f_v to get the desired droplets.

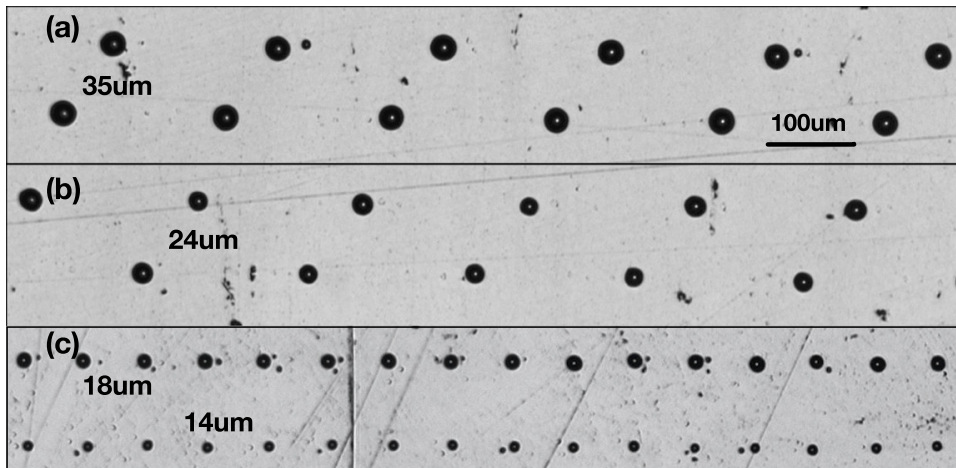


Figure 11. Fine droplets arrays of four different diameters are printed with the help of control equation. Voltage is 2 kV, nozzle is 34 G. The smallest droplets are printed at 18 nl min⁻¹; others are at 180 nl min⁻¹.

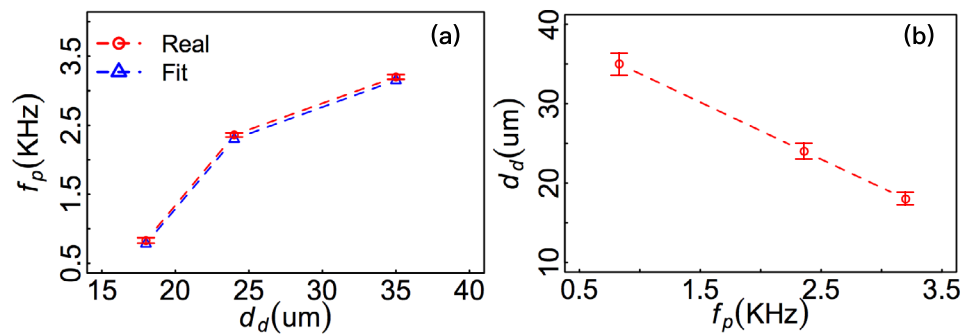


Figure 12. Comparison of printing frequency between estimated values and actual values, and the print accuracy based on figure 10: (a) estimated printing frequency compared with actual printing frequency; (b) accuracy of droplet diameter.

A simple method can be used to get desired droplet spacing with the help of the droplet diameter control equations. As shown in figure 11, droplets with the diameter of 35 μm and 24 μm are arranged at the same spacing, and the spacing between every pair of droplets with the diameter of 18 μm and 14 μm is also the same. To make droplet arrays with different sizes have the same droplet spacing, we set the moving stage velocity in the X direction as U_x , combine the estimated printing frequencies calculated from droplet size control equations, and provide equation (7) for controlling droplet space S_d :

$$S_d = \frac{U_{x1}}{f_{p1}} = \frac{U_{x2}}{f_{p2}}. \quad (7)$$

Figure 12 presents the comparison of printing frequency and the verification of print accuracy based on print results in figure 11. As shown in figure 12(a), the actual printing frequencies in figure 11 are 820 Hz, 2.36 kHz and 3.23 kHz, which are slightly larger than the estimated printing frequencies. However, the difference between these frequencies is small enough to ensure that the droplet diameter parameter control is valuable for high frequency pulsed EHD printing. In addition, referring to figure 12(b), we analyzed the print accuracy of droplet diameter. It can be seen that the droplet diameter accuracy increases as the droplet diameter decreases or the printing frequency increases, which proves our method can achieve high precision printing with high efficiency.

Figure 13 shows the print ability of high pulsed EHD printing based on parameter control. In figure 13, from top to bottom, the diameters of four printed droplets lines are 21 μm, 24 μm, 26 μm and 28 μm. In each row, the diameters of printed droplets are close to each other with very small size error. Taking into account that the diameters of printed droplets demonstrated in figure 13 are larger than 16 μm–18 μm, 30 G–180 nl min⁻¹ should be selected for printing. According to the droplet size study and equation (5), the estimated printing frequencies of four droplet sizes can be calculated, which are 2727 Hz, 2311 Hz, 2033 Hz and 1755 Hz. In real printing processes, the printing frequencies are approximately 2790 Hz, 2285 Hz, 2010 Hz and 1780 Hz. The error between the estimated value and the actual value of printing frequency is less than 5%, indicating that the droplet size control equation can guide the printing process. In addition, in order to achieve a better droplet lattice effect, we tried to keep the spacing between adjacent droplets in one row at 20 μm. Moving stage velocities are set by reference to equation (7). According to figure 13, the droplet spacing of the first row is approximately 19 μm (error less than 5%), and the droplet spacing of the following three rows of droplets is approximately 17 μm–18 μm (error close to 10%). The large droplet spacing error of large droplets may be due to the larger inertial force caused by larger droplets under the same moving stage velocity dragging, which results in a larger centroid

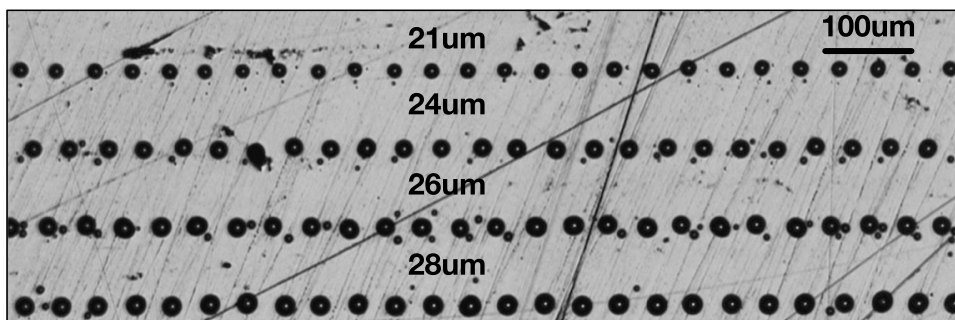


Figure 13. Four printed droplet arrays with increasing size from 21 μm to 28 μm via high frequency pulsed EHD printing. Flow rate–nozzle is 180 nl min^{-1} –30 G, voltage is 2 kV, and duty cycle is 50%. Spacing between every two droplets is set as 20 μm . The detailed voltage frequencies are estimated by equation

deviation of the final droplet shape. Furthermore, as shown in figure 13, some extremely small droplets are found next to printed droplets. This may be because the close arrangement of printed droplets makes partial charges carried by droplets remain on the substrate, which easily leads to the deviation and fragmentation of the ejected jet, resulting in the formation of associated small droplets [7, 26].

6. Conclusion

In this paper, we have studied the influence of external parameters, such as flow rate, nozzle diameter and duty cycle, on pulsed EHD printing, and introduced a droplet size printing method with high printing frequency based on parameter control. For high frequency pulsed EHD printing, the parameters grouping of flow rate and duty cycle is the key factor to the printing performance (printing frequency and droplet size). Large flow rate with moderate duty cycle, such as 180 nl min^{-1} –50%, enables the meniscus at high voltage frequency to form a stable stimulated oscillation, bringing the maximal printing frequency f_{pmax} up to 3.5 kHz. Nozzle diameter, voltage and conductivity all affect f_{pmax} , i.e. f_{pmax} increases with decreased nozzle diameter and increased voltage, and a large effective voltage range of f_{pmax} can be achieved by using a nozzle with moderate diameter (30 G).

With large flow rate and moderate duty cycle, droplet diameter d_d decreases steadily with voltage f_v , which is beneficial for droplet size control. By choosing small flow rate with small voltage-sensitive nozzle, such as 18 nl min^{-1} –34 G, extremely fine droplets can be obtained. We also found that voltage change has little effect on droplet size when flow rate and nozzle size are both small. However, when flow rate is large and nozzle size is small (such as 180 nl min^{-1} –32 G or 34 G), smaller voltage (1.8 kV) can stimulate the meniscus to form smaller droplets at high frequency voltage.

We established parameter equations to flexibly control droplet size. Droplets with minimal diameter of 16 μm –18 μm can be achieved using 30 G (ID 160 μm), where the nozzle-to-droplet ratio is close to 10. Droplets with minimal diameter of about 8 μm can be achieved using 34 G (ID 60 μm), and the printing frequency can reach 1.5 kHz–3 kHz, or even higher.

We verified this method by demonstrating the printing results of different droplets sizes and spaces, and examining

the accuracy of droplet size and the effectiveness of the control method. In future work, the interaction between droplet and substrate will be studied along with the influence of parameters on position error of droplet spacing, to further improve the efficiency and accuracy of this method.

Acknowledgments

This work is supported in part by the National Natural Science Foundation of China under Grant 51175344, the ‘Shu Guang’ Program of Shanghai Municipal Education Commission and Shanghai Education Development Foundation under Grant 11SG14.

ORCID iDs

Xin Yuan  <https://orcid.org/0000-0002-5540-5131>

References

- [1] Alexander M S, Paine M D and Stark J P 2006 Pulsation modes and the effect of applied voltage on current and flow rate in nanoelectrospray *Anal. Chem.* **78** 2658–64
- [2] Muhammad N M, Sundharam S, Dang H-W, Lee A, Ryu B-H and Choi K-H 2011 Cis layer deposition through electrospray process for solar cell fabrication *Curr. Appl. Phys.* **11** S68–75
- [3] Chakraborty S, Liao I-C, Adler A and Leong K W 2009 Electrohydrodynamics: a facile technique to fabricate drug delivery systems *Adv. Drug. Deliv. Rev.* **61** 1043–54
- [4] Siringhaus H, Kawase T, Friend R, Shimoda T, Inbasekaran M, Wu W and Woo E 2000 High-resolution inkjet printing of all-polymer transistor circuits *Science* **290** 2123–6
- [5] de Gans B-J, Duineveld P C and Schubert U S 2004 Inkjet printing of polymers: state of the art and future developments *Adv. Mater.* **16** 203–13
- [6] Calvert P 2001 Inkjet printing for materials and devices *Chem. Mater.* **13** 3299–305
- [7] Wei C, Qin H, Ramírez-Iglesias N A, Chiu C-P, Lee Y-s and Dong J 2014 High-resolution ac-pulse modulated electrohydrodynamic jet printing on highly insulating substrates *J. Micromech. Microeng.* **24** 045010
- [8] Chen C-H, Saville D and Aksay I 2006 Scaling laws for pulsed electrohydrodynamic drop formation *Appl. Phys. Lett.* **89** 124103

- [9] Lee M, Kang D, Kim N, Kim H, James S and Yoon S 2012 A study of ejection modes for pulsed-dc electrohydrodynamic inkjet printing *J. Aerosol Sci.* **46** 1–6
- [10] Juraschek R and Röhlgen F 1998 Pulsation phenomena during electrospray ionization *Int. J. Mass Spectrom.* **177** 1–15
- [11] Ganan-Calvo A, Rebollo-Munoz N and Montanero J 2013 The minimum or natural rate of flow and droplet size ejected by Taylor cone-jets: physical symmetries and scaling laws *New J. Phys.* **15** 033035
- [12] Park J-U *et al* 2007 High-resolution electrohydrodynamic jet printing *Nat. Mater.* **6** 782
- [13] Barton K, Mishra S, Alleyne A, Ferreira P and Rogers J 2011 Control of high-resolution electrohydrodynamic jet printing *Control Eng. Pract.* **19** 1266–73
- [14] Chen C-H, Saville D and Aksay I 2006 Electrohydrodynamic drop-and-place particle deployment *Appl. Phys. Lett.* **88** 154104
- [15] Wang K and Stark J 2010 Deposition of colloidal gold nanoparticles by fully pulsed-voltage-controlled electrohydrodynamic atomisation *J. Nanoparticle Res.* **12** 707–11
- [16] Byun D, Nguyen V D, Dutta P and Park H C 2010 A hybrid inkjet printer utilizing electrohydrodynamic jetting and piezoelectric actuation *Jpn. J. Appl. Phys.* **49** 060216
- [17] Kim J, Oh H and Kim S S 2008 Electrohydrodynamic drop-on-demand patterning in pulsed cone-jet mode at various frequencies *J. Aerosol Sci.* **39** 819–25
- [18] Xu L and Sun D 2013 Electrohydrodynamic printing under applied pole-type nozzle configuration *Appl. Phys. Lett.* **102** 024101
- [19] Kang D, Lee M, Kim H, James S and Yoon S 2011 Electrohydrodynamic pulsed-inkjet characteristics of various inks containing aluminum particles *J. Aerosol Sci.* **42** 621–30
- [20] Mishra S, Barton K L, Alleyne A G, Ferreira P M and Rogers J A 2010 High-speed and drop-on-demand printing with a pulsed electrohydrodynamic jet *J. Micromech. Microeng.* **20** 095026
- [21] Shigeta K, He Y, Sutanto E, Kang S, Le A-P, Nuzzo R G, Alleyne A G, Ferreira P M, Lu Y and Rogers J A 2012 Functional protein microarrays by electrohydrodynamic jet printing *Anal. chem.* **84** 10012–8
- [22] Wang K, Paine M D and Stark J P 2009 Freeform fabrication of metallic patterns by unforced electrohydrodynamic jet printing of organic silver ink *J. Mater. Sci.: Mater. Electron.* **20** 1154–7
- [23] Prasetyo F D, Yulistira H T, Nguyen V D and Byun D 2012 Morphologies of Ag dots printed by electrohydrodynamic (ehd) jet printing on a silicon wafer *12th Int. Conf. on Control, Automation and Systems (IEEE)* pp 389–91
- [24] Choi H K, Park J-U, Park O O, Ferreira P M, Georgiadis J G and Rogers J A 2008 Scaling laws for jet pulsations associated with high-resolution electrohydrodynamic printing *Appl. Phys. Lett.* **92** 123109
- [25] Yulistira H T, Nguyen V D, Dutta P and Byun D 2010 Flight behavior of charged droplets in electrohydrodynamic inkjet printing *Appl. Phys. Lett.* **96** 023503
- [26] Yulistira H T, Nguyen V D, Tran S B Q, Kang T S, Park J K and Byun D 2011 Retreat behavior of a charged droplet for electrohydrodynamic inkjet printing *Appl. Phys. Lett.* **98** 083501
- [27] Choi J, Kim Y-J, Lee S, Son S U, Ko H S, Nguyen V D and Byun D 2008 Drop-on-demand printing of conductive ink by electrostatic field induced inkjet head *Appl. Phys. Lett.* **93** 193508
- [28] Marginean I, Parvin L, Heffernan L and Vertes A 2004 Flexing the electrified meniscus: the birth of a jet in electrosprays *Anal. Chem.* **76** 4202–7
- [29] Marginean I, Nemes P, Parvin L and Vertes A 2006 How much charge is there on a pulsating Taylor cone? *Appl. Phys. Lett.* **89** 064104
- [30] Paine M D, Alexander M S and Stark J P 2007 Nozzle and liquid effects on the spray modes in nanoelectrospray *J. Colloid Interface Sci.* **305** 111–23
- [31] Stachewicz U, Dijkstra J F, Yurteri C U and Marijnissen J C 2007 Experiments on single event electrospraying *Appl. Phys. Lett.* **91** 254109
- [32] Yuan X, Ba Z and Xiong Z 2015 Fine droplet generation using tunable electrohydrodynamic pulsation *J. Micromech. Microeng.* **25** 075028
- [33] Deng W and Gomez A 2012 Full transient response of Taylor cones to a step change in electric field *Microfluidics Nanofluidics* **12** 383–93
- [34] Gañán-Calvo A M 1999 The surface charge in electrospraying: its nature and its universal scaling laws *J. Aerosol Sci.* **30** 863–72
- [35] Castro-Hernández E, García-Sánchez P, Tan S H, Gañán-Calvo A M, Baret J-C and Ramos A 2015 Breakup length of ac electrified jets in a microfluidic flow-focusing junction *Microfluidics Nanofluidics* **19** 787–94
- [36] Chen I-M, Tsai H-H, Chang C-W, Zheng G and Su Y-C 2018 Electric-field triggered, on-demand formation of sub-femtoliter droplets *Sensors Actuators B* **260** 541–53
- [37] Tan S H, Semin B and Baret J-C 2014 Microfluidic flow-focusing in ac electric fields *Lab Chip* **14** 1099–106
- [38] Choi K-H, Ali K and Rahman K 2014 A study of the dependence of electrohydrodynamic jetting on the process parameters and liquid physical properties *Chin. J. Phys.* **52** 799–815
- [39] Barrero A, Ganan-Calvo A, Davila J, Palacios A and Gomez-Gonzalez E 1999 The role of the electrical conductivity and viscosity on the motions inside Taylor cones *J. Electrostat.* **47** 13–26
- [40] Tan S H, Maes F, Semin B, Vignon J and Baret J-C 2014 The microfluidic jukebox *Sci. Rep.* **4** 4787
- [41] Xi H-D, Guo W, Leniart M, Chong Z Z and Tan S H 2016 Ac electric field induced droplet deformation in a microfluidic t-junction *Lab Chip* **16** 2982–6